Hydrodynamic simulations of relativistic heavy-ion collisions with different calculations of the QCD equation of state

J. Scott Moreland[1] and Ron A. Soltz[2]

[1]*Department of Physics, Duke University, Durham, NC 27708-0305*
[2]*Lawrence Livermore National Laboratory, Livermore, CA 94551-0808*

(Dated: August 19, 2015)

I. INTRODUCTION

Fluid dynamics is a useful framework to study the collective behaviour of hot and dense nuclear matter produced in relativistic heavy-ions. Quantum Chromodynamics (QCD) predicts that at sufficiently high energies these collisions form a new state of matter consisting of deconfined quarks and gluons known as a quark-gluon plasma (QGP). Simulations based on relativistic viscous hydrodynamics play a central role in extracting properties of the QGP which expands and freezes into hadrons too quickly for direct observation.

The hydroynamic transport equations require two essential ingredients to specify the full time evolution of the QGP fireball: initial conditions which describe the thermal profile of the QGP droplet at some early starting time and a QCD equation of state which interrelates energy density, pressure and temperature of each fluid cell in local thermal equillibrium.

Lattice discretization is the only reliable method to calculate the QCD equation of state in the vicinity of the QGP phase transition and hence constitutes a critical component of hydrodynamic simulations. While lattice techniques are rigorous in their treatment of the underlying QCD Lagrangian, they are subject to numerical errors inherent in the lattice discretization procedure. These errors are manifest in differences in the continuum extrapolated QCD trace anomaly predicted by different lattice collaborations and lead to an overall uncertainty in the true value of the QCD equation of state at zero baryochemical potential.

Simulations using a lattice based equation of state inherrit all forms of numeric and systematic uncertainty associated with the underlying lattice methodology. These modeling uncertainties have been studied both at low temperature, by comparing simulations with a lattice equation of state to results obtained from a hadron resonance gas model [1], and at high temperature by comparing the effect of different lattice parameterizations of the lattice equation of state on particle spectra and flow [1, 2].

Recent calculations by the HotQCD and Wuppertal-Budapest collaborations of the QCD trace anomaly in the continuum limit now show good agreement within errors. This signals an important convergence in lattice descriptions of the QCD equation of state which previously exhibited a tension in the peak of the trace anomaly near the QGP phase transition. It is not yet clear however, if current lattice errors are under sufficient control for hydrodynamic transport models or if further improvement is needed.

In this work, we quantify the effect of lattice errors on simulations of relativistic heavy-ion collisions by comparing simulation predictions obtained with different calculations of the QCD equation of state. The equations of state are analyzed using a modern event-by-event hybrid simulation which couples viscous hydrodynamics to a hadronic afterburner to calculate flows, spectra and Bertsch-Pratt radii and are compared to measurements at the Relativistic Heavy-Ion Collider (RHIC).

We analyze two state of the art calculations from the HotQCD and Wuppertal-Budapest collaborations as well as an older parameterization based on HotQCD calculations with a coarser lattice spacing to gauge the importance of recent lattice improvements. We also assess the need for additional improvements to the current state of the art by sampling equation of state curves from the latest HotQCD published errors to quantify current uncertainties.

II. EQUATIONS OF STATE

The hybrid simulation used in this work switches from viscous hydrodynamics to a microscopic kinetic description once the system expands, cools and freezes into hadrons. While the QCD equation of state enters the hydrodynamic phase of the simulation as a freely specified function interrelating energy density, pressure and temperature, its description in the kinetic phase of the collision is fixed by the finite number of particles and particle resonances included in the UrQMD model used for the hadronic phase of the simulation.

As a result, we limit our study to differences in the QCD equation of state *above* the QGP transition temperature where hydrodynamics allows us to freely vary its chosen form. We study three different parameterizations for this high temperature dependence – two state of the art calculations in 2+1 flavour QCD from the HotQCD [3] and Wuppertal-Budapest [4] collaborations, as well as the older s95p-v1 parameterization [1] constructed using lattice data measured with a coarser lattice spacing [5].

The QCD equation of state is frequently characterized by the trace of the energy-momentum tensor, also referred to as the trace anomaly or interaction measure. When scaled by powers of the temperature, the trace anomaly forms a dimensionless measure

$$I \equiv \frac{\Theta^{\mu\mu}(T)}{T^4} = \frac{e-3p}{T^4}, \tag{1}$$

where e is the local fluid energy density, p the pressure and T the temperature.

In Fig. 1 we plot the temperature scaled interaction measure of each equation of state as well as that of a hadron resonance gas calculated from the list of partial resonances included in the UrQMD collision kernel. The s95p-v1 parameterization, which was constructed to interpolate between a hadron resonance gas calculation at low temperatures and lattice results at high temperatures, is in good agreement with the UrQMD equation of state while the HotQCD and Wuppertal-Budapest results are slightly higher in the vicinity of the phase transition.

To ensure a self consistent description in regions of the collision where the simulation switches from hydrodynamics to Boltzmann transport, we match each high temperature lattice equation of state with the low temperature UrQMD equation of state. We thus define a piecewise function for the temperature scaled interaction measure,

$$I(T) = \begin{cases} I_{\mathrm{hrg}}(T) & T \leq T_1 \\ I_{\mathrm{blend}}(T) & T_1 < T < T_2 \\ I_{\mathrm{lattice}}(T) & T \geq T_2, \end{cases} \tag{2}$$

where I_{hrg} is the hadron resonance gas trace anomaly in UrQMD pictured in Fig. 1, I_{lattice} represents one of the HotQCD, Wuppertal-Budapest or S95p-v1 parameterizations and I_{blend} is a function which smoothly connects between the two in the temperature interval $T_1 < T < T_2$,

$$I_{\mathrm{blend}} = (1-z)\, I_{\mathrm{hrg}} + z\, I_{\mathrm{lattice}}. \tag{3}$$

The interpolation parameter $z \in [0, 1]$ in equation 3 is constructed to match the first and second derviatives at the endpoints of the interpolation interval,

$$z = 6x^5 - 15x^4 + 10x^3 \tag{4}$$

$$\text{where } x = (T - T_1)/(T_2 - T_1), \tag{5}$$

where the endpoints $T_1 = T_{\mathrm{sw}}$ and $T_2 = 180$ MeV smoothly interpolate the lattice results into the UrQMD trace anomaly at the desired switching temperature T_{sw}.

In principle, the switching temperature could assume any value in a small interval below the equation of state's pseudo-critical transition temperature T_{c} and should be tuned to fit the relative abundance of pions, protons and kaons measured by experiment. Since we are primarily interested in the sensitivity of the simulation to changes in the equation of state with all other quantities held fixed, we fix the transition temperature using the HotQCD chiral transition temperature $T_{\mathrm{sw}} = T_{\mathrm{c}} = 154$ MeV.

The modified interaction measures, labeled with a prime to distinguish them from the raw lattice results, are plotted in Fig. 2. The vertical gray line marks the hydro-to-micro switching temperature $T_{\mathrm{sw}} = 154$ MeV where the model switches from the VISH2+1 hydrodynamics code to UrQMD.

In Fig. 3 we plot the squared speed of sound $c_s^2 = dp/de$ for each modified interaction measure. The speed of sound of the HotQCD' and WB' equations of state are in good agreement while the S95' parameterization remains softer in a wider interval about the QGP phase transition. We note that the speed of sound in the HotQCD' and WB' parameterizations is clearly affected by the parametric transition (3) in the vicinity of the switching temperature (vertical gray line), but that the imposed matching maintains continuity.

With the trace anomalies in hand, the energy density, pressure and entropy density are easily interrelated to specify the equation of state used in the analysis,

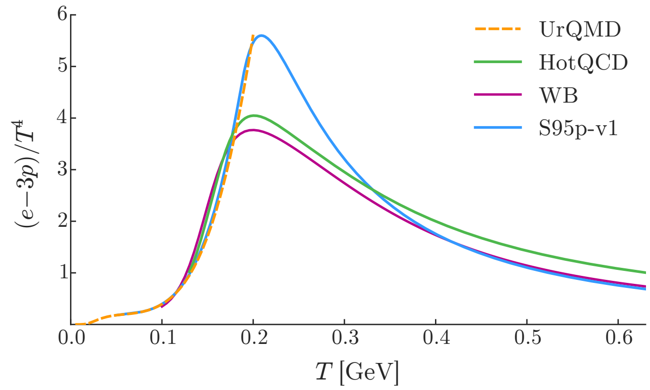

FIG. 1. The temperature scaled QCD trace anomaly for the UrQMD. HotQCD, WB and s95p-v1 parameterizations as a function of temperature [?].

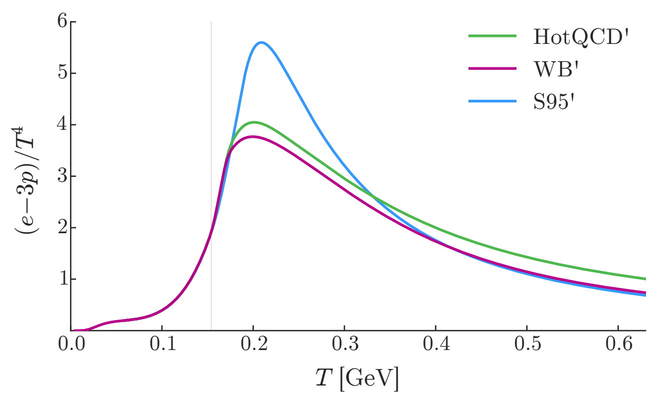

FIG. 2. The modified QCD trace anomalies HotQCD', WB' and S95' obtained from equation (2) and the corresponding lattice parameterizations in Fig. 1. The gray, vertical line marks the hydro-to-micro switching temperature $T_{\mathrm{sw}} = 154$ MeV.

$$\frac{p(T)}{T^4} = \int_0^T dT' \, \frac{I(T')}{T'}, \tag{6}$$

$$\frac{e(T)}{T^4} = I(T) + 3\,\frac{p(T)}{T^4}, \tag{7}$$

$$\frac{s(T)}{T^3} = \frac{e(T)+p(T)}{T^4}. \tag{8}$$

III. HYBRID MODEL

The equations of state are embedded in the modern event-by-event VISHNU hybrid model which uses the VISH2+1 boost-invariant viscous hydrodynamics code to simulate the time evolution of the QGP medium and a microscopic UrQMD hadronic afterburner for subsequent evolution below the QGP transition temperature. Where necessary, free parameters of the model are are tuned to facillitate model-to-data comparison with 200 GeV gold-gold collisions at RHIC. In this section, we briefly outline the implementation of the model used in the analysis; for a more detailed explanation of the VISHNU model, we refer the reader to [].

A. Initial conditions

The hydrodynamic initial conditions are generate using a Monte Carlo Glauber model based on a common two-component ansatz which deposits entropy proportional to a linear combination of nucleon participants and binary nucleon-nucleon collisions,

$$dS/dy\,|_{y=0} \propto \frac{(1-\alpha)}{2} N_{\mathrm{part}} + \alpha N_{\mathrm{coll}} \tag{9}$$

where for the binary collision fraction, we use $\alpha = 0.14$ which has been shown to provide a good description of the centrality dependence of charged particle multiplicity in 200 GeV gold-gold collisions [?].

The entropy is localized about each nucleon's transverse parton density $T_p(\mathbf{x})$,

$$\begin{aligned} dS/dy\,|_{y=0} \propto &\sum_{i=0}^{N_{\mathrm{part,A}}} w_i\, T_p(\mathbf{x}-\mathbf{x}_i)(1-\alpha+\alpha\, N_{\mathrm{coll,i}}) \\ &+ \sum_{j=0}^{N_{\mathrm{part,B}}} w_j\, T_p(\mathbf{x}-\mathbf{x}_i)(1-\alpha+\alpha\, N_{\mathrm{coll,j}}) \end{aligned} \tag{10}$$

where the summations run over the participants in each nucleus, $N_{\mathrm{coll,i}}$ denotes the number of binary collisions suffered by the i^{th} nucleon and the proton density $T_p(\mathbf{x})$ is described by a Gaussian

$$T_p(\mathbf{x}) = \frac{1}{\sqrt{2\pi B}} \exp\left(-\frac{x^2+y^2}{2B}\right) \tag{11}$$

with transverse area $B = 0.36$ fm^2.

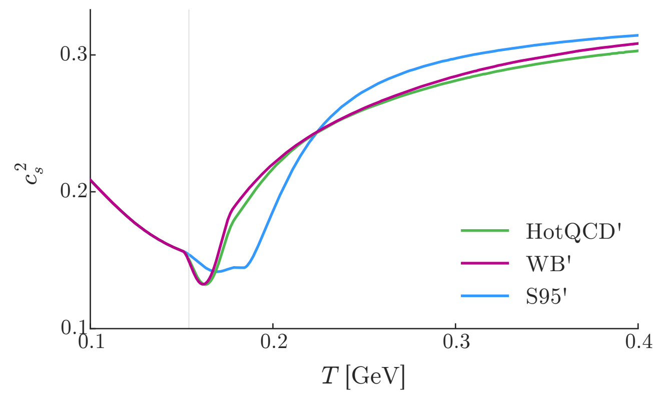

FIG. 3. Speed of sound squared c_s^2 plotted versus temperature T for the three equations of state used in this study. The vertical gray line indicates the switching temperature $T_{\mathrm{sw}} = 154$ MeV where the model switches from fluid dynamics to a microscopic transport model.

The random nucleon weights w_i in equation (10) are sampled independently from a Gamma distribution with unit mean

$$P_k(w) = \frac{k^k}{\Gamma(k)} w^{k-1} e^{-kw}, \tag{12}$$

and shape parameter $k = \mathrm{Var}(P)^{-1}$ which modulates the variance of the distribution. These fluctuations are typically added [?] to reproduce the large multiplicity fluctuations observed in minimum bias proton-proton collisions. In this work the shape parameter is fixed to $k = 1$ determined by a fit to the 200 GeV UA5 data [?].

The initial condition profiles, which provide the entropy density $dS/(d^2r_\perp\, d\eta\, \tau_{\mathrm{therm}})$ at the QGP thermalization time, are finally rescaled by an overall normalization factor to fit the measured charged particle multiplicity in 0–10% centrality collisions.

B. Hydrodyamics and Boltzmann transport

The hydrodynamic equations of motion are obtained in VISHNew by solving the second-order Israel-Stewart equations,

$$\partial_\mu T^{\mu\nu} = 0, \quad T^{\mu\nu} = e u^\mu u^\nu - (p+\Pi)\Delta^{\mu\nu} + \pi^{\mu\nu}, \tag{13}$$

where the bulk pressure Π and shear stress $\pi^{\mu\nu}$ satisfy the relaxation equations,

$$\mathcal{D}\Pi = -\frac{1}{\tau_\Pi}(\Pi + \zeta\theta) - \frac{1}{2}\Pi \frac{\zeta T}{\tau_\Pi} d_\lambda \left(\frac{\tau_\Pi}{\zeta T} u^\lambda\right),$$

$$\Delta^{\mu\alpha}\Delta^{\nu\beta}\mathcal{D}\pi_{\alpha\beta} = -\frac{1}{\tau_\pi}(\pi^{\mu\nu} - 2\eta\sigma^{\mu\nu}) \tag{14}$$

$$-\frac{1}{2}\pi^{\mu\nu}\frac{\eta T}{\tau_\pi} d_\lambda \left(\frac{\tau_\pi}{\eta T} u^\lambda\right). \tag{15}$$

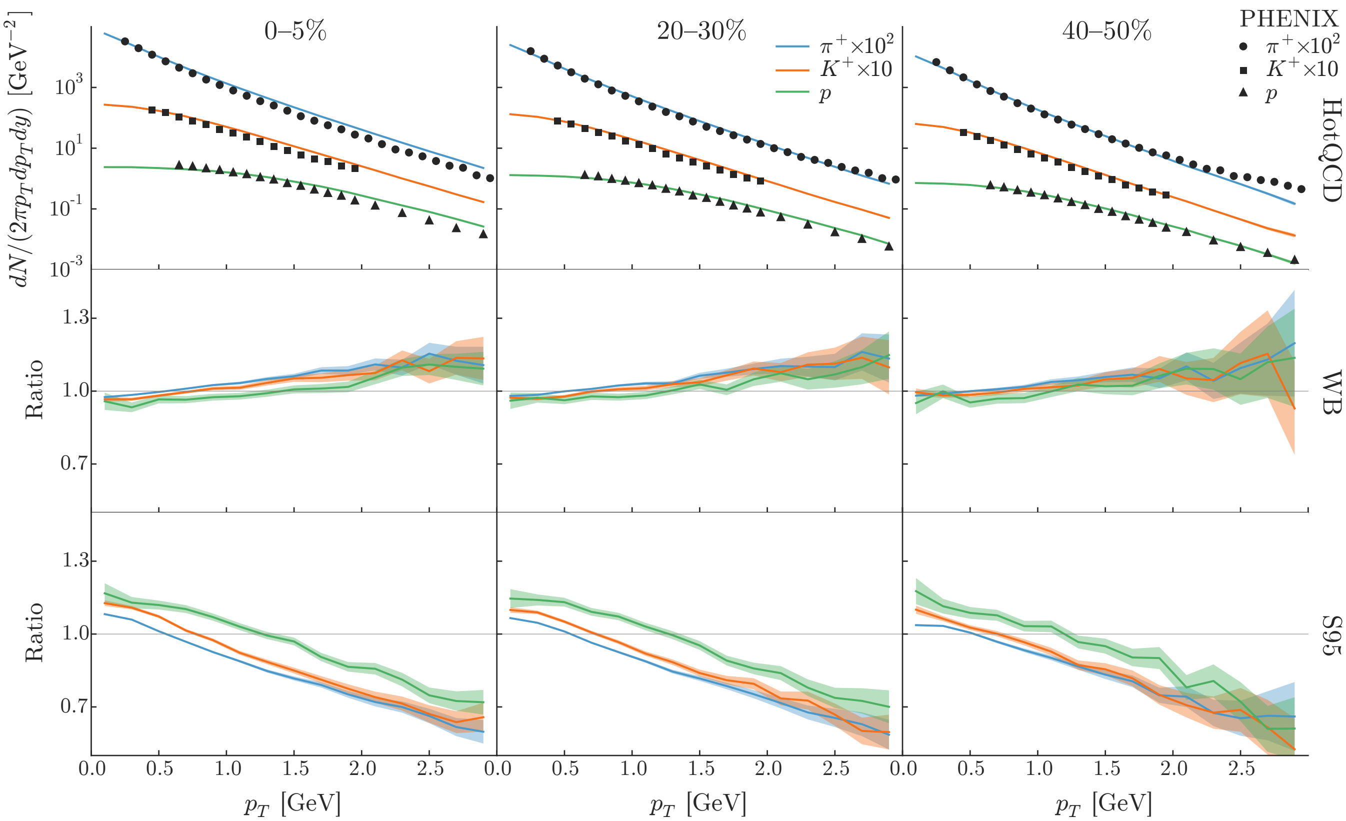

FIG. 4. Effect of the equation of state on transverse momentum spectra. Top row: model calculations using the HotQCD equation of state plotted against PHENIX data for pions, kaons and protons (blue lines/circles, red lines/squares and green lines/triangles) in centrality bins 0–5%, 20–30% and 40–50% (columns left to right). Middle and bottom rows: ratios of the WB' and S95' invariant yields to the HotQCD' result. Shaded bands indicate two sigma statistical error.

We follow the work in reference [?] and fix the bulk viscosity ζ and shear viscosity η in equation (14) using a constant specific shear viscosity $\eta/s = 0.08$ and vanishing bulk viscosity $\zeta/s = 0$ in the hydrodynamic phase of the simulation. It would be interesting to study the effect of bulk viscous corrections which are sensitive to the peak of the QCD trace anomaly near the QGP phase transition [?]. Unfortunately, bulk viscous corrections do not have a straight forward implementation in the present hybrid model and are neglected in this work.

As previously explained in section II, the VISHNU hybrid model transitions from hydrodyamic field equations to microscopic transport at a sudden switching temperature $T_{\rm sw}$ at which the hydrodynamic energy-momentum tensor is particlized using the Cooper-Frye freezeout prescription,

$$E\frac{dN_i}{d^3p} = \int_\sigma f_i(x,p)p^\mu d^3\sigma_\mu \tag{16}$$

where f_i is the distribution function of particle species i, p^μ is its four-momentum and $d^3\sigma_\mu$ characterizes an element of the isothermal freezeout hypersurface defined by $T_{\rm sw}$.

The sampled particles then enter the UrQMD simulation where the Boltzmann equation,

$$\frac{df_i(x,p)}{dt} = \mathcal{C}_i(x,p), \tag{17}$$

is solved to simulate all elastic and inelastic collisions between the particles with collision kernel $\mathcal{C}_i$ until the system becomes too dillute to continue interacting. Finally, the four-position, four-momentum and particle identification number of each particle recorded at the moment of last interaction.

IV. RESULTS

The results section is organized as follows. In subsection IV A we calculate the particle spectra for each equation of state across three different centrality classes using the final particle information output by the hybrid simulation. In sub-section IV B we repeat the calculation for elliptic and triangular flow but perform the calculation on the hydrodynamic Cooper-Frye freezeout surface for reasons explained later in the text. In subsection 20 we calculate the femptoscopic event-averaged Bertsch-Pratt radii, again using the final particle infor-

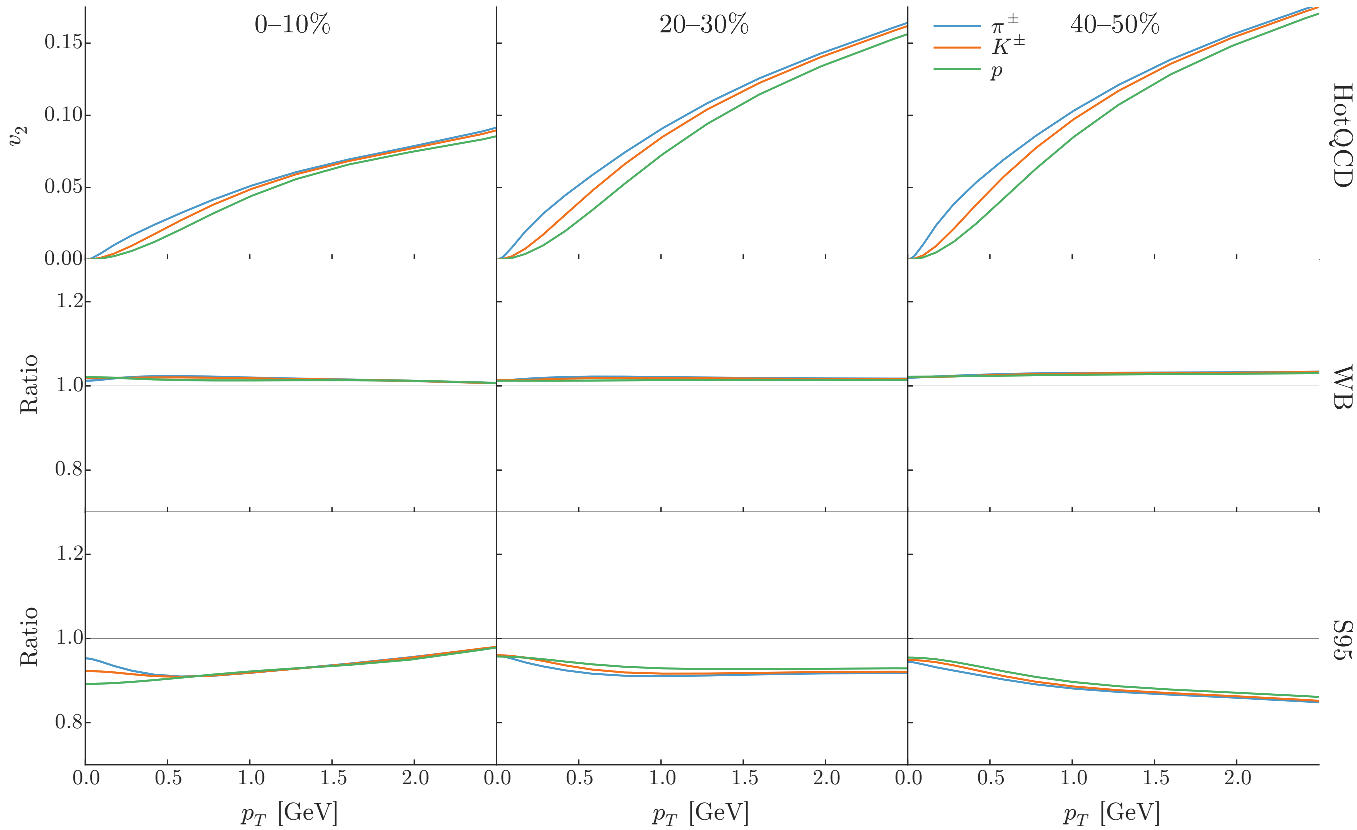

FIG. 5. Effect of the equation of state on differential elliptic flow $v_2(p_T)$ calculated from the Cooper-Frye freezeout hypersurface (19). Top row: model calculations using the HotQCD' equation of state for the elliptic flow $v_2(p_T)$ of pions, kaons and protons (blue, orange and green lines) in centrality bins 0–10%, 20–30% and 40–50% (columns left to right). Middle and bottom rows: ratios of the WB' and S95' elliptic flow to the HotQCD' result. Statistical errors are smaller than the linewidth and have been omitted.

mation output by the full hybrid calculation. Finally in sub-section IV D, we repeat the spectra and flow analysis using a sampling of equation of state curves from the HotQCD published errors.

All results presented in the following sections are based on 10^5 minimum bias events which are subdivided into centrality classes according to initial entropy, e.g. the initial condition events with 20% highest entropy comprise centrality class 0–20%. Each hydrodynamic event is oversampled an additional four times to increase the number of particles in each event and suppress finite statistical error.

A. Particle spectra

Figure 4 shows the invariant yield $dN/(2\pi p_T dp_T dy)$ of positively charged pions, kaons and protons calculated from the hybid model for the 0–5%, 20–30% and 40–50% centrality classes using the HotQCD', WB' and S95' equations of state constructed in section II.

The first row shows the HotQCD' yields obtained from the hybrid model plotted against observed pion, proton and kaon data from PHENIX. The second and third rows show the ratio of the invariant yields of the WB' and S95' equations of state over the the HotQCD' result. We see that the HotQCD' equation of state provides a good description of observed particle yields except for at moderate to large p_T in central collisions where the equation of state overpredicts the data. This agreement would likely improve with more realistic initial conditions, bulk viscous corrections and/or more careful treatment of the hydro-to-micro switching temperature T_{sw}, and thus we defer from making any specific conclusions from the overall fit to data. It suffices to say that the most recent HotQCD lattice results provide a reasonable description of the PHENIX data and agrees within the overall uncertainty of the present model.

Looking at the second and third rows of the figure which show the ratios of the WB' and S95' yields to the HotQCD' result, we see that the spectra predicted by the HotQCD' and WB' equations of state agree within statistical error, while the S95' equation of state is appreciably softer and produces $\sim 10\%$ more particles at $p_T = 0.5$ GeV and $\sim 30\%$ fewer particles at $p_T = 2.5$ GeV across all three centralities.

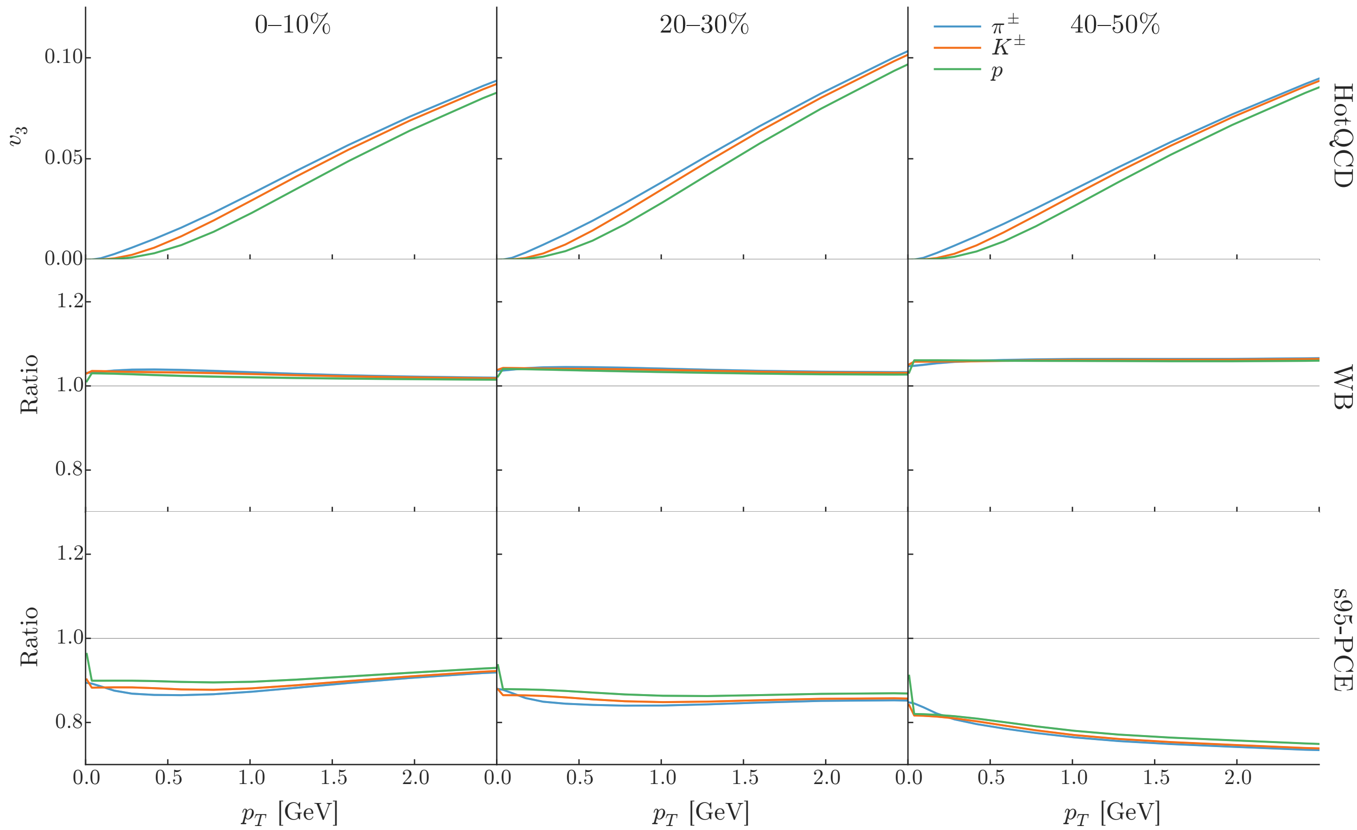

FIG. 6. Same as Fig. 5 but for differential triangular flow $v_3(p_T)$. Note that the y-axis limits in the top row are different.

B. Elliptic and triangular flows

The azimuthal anisotropy of final particle emission is characterized by the Fourier expansion

$$E\frac{d^3N}{d^3p} = \frac{1}{2\pi}\frac{d^2N}{dyp_Tdp_T}\left(1 + \sum_{n=1}^{\infty} 2v_n \cos n(\phi - \Psi_{RP})\right) \quad (18)$$

where ϕ is the direction of the emitted particle, Ψ_{RP} is the reaction plane angle of the event and v_n the anisotropic flow coefficient corresponding to the Fourier harmonic of order n.

The reaction plane angle cannot be measured experimentally and the anisotropic flow is typically estimated using multi-particle correlations such as two and four-particle cumulants. The statistical error of the event-averaged estimators is suppressed with both increasing event multiplicity and event sample size. This can pose a challenge for computationally intensive hybrid model calculations which typically cannot reach integrated luminosities comparable to experiment.

Statistical errors are particularly noxious in differential flow calculations at moderate to large p_T where particle statistics are limited. We circumvent this issue in the differential flow analysis and calculate the flow anisotropy of pions, kaons and protons directly from the Cooper-Frye freezeout surface using the built in routines in the VISHNU package according to

$$v_n(p_T) = \frac{\int d\phi_p e^{in\phi_p} dN/(dyp_Tdp_Td\phi_p)}{\int d\phi_p\, dN/(dyp_Tdp_Td\phi_p)}. \quad (19)$$

Consequently, the present flow sensitivity analysis does not include contributions from flow generated by the UrQMD hadronic afterburner which is indentical for each of the three equations of state. Hence, the following results should be interpretted as a conservative *upper* bound on the goodness of fit sensitivity expected in a full hybrid model simulation.

Figs. 5 shows the elliptic flow v_2 of pions, kaons and protons calculated from equation (19) for the HotQCD', WB' and S95' equations of state in 0–10, 20–30 and 40–50% centrality bins. The first row of the figure shows the elliptic flow predicted by the HotQCD' equation of state while the middle and bottom rows display theoretical ratios of the WB' and S95' predictions over the HotQCD' result. The information in Fig. 6 is identical to that in Fig. 5 except that elliptic flow v_2 has been replaced with triangular flow v_3.

We see in Fig. 5 that the elliptic flow generated by the HotQCD' and WB' parameterizations is in very good agreement across all centralities, while the S95' parameterization systematically generates $\sim 10\%$ less flow than

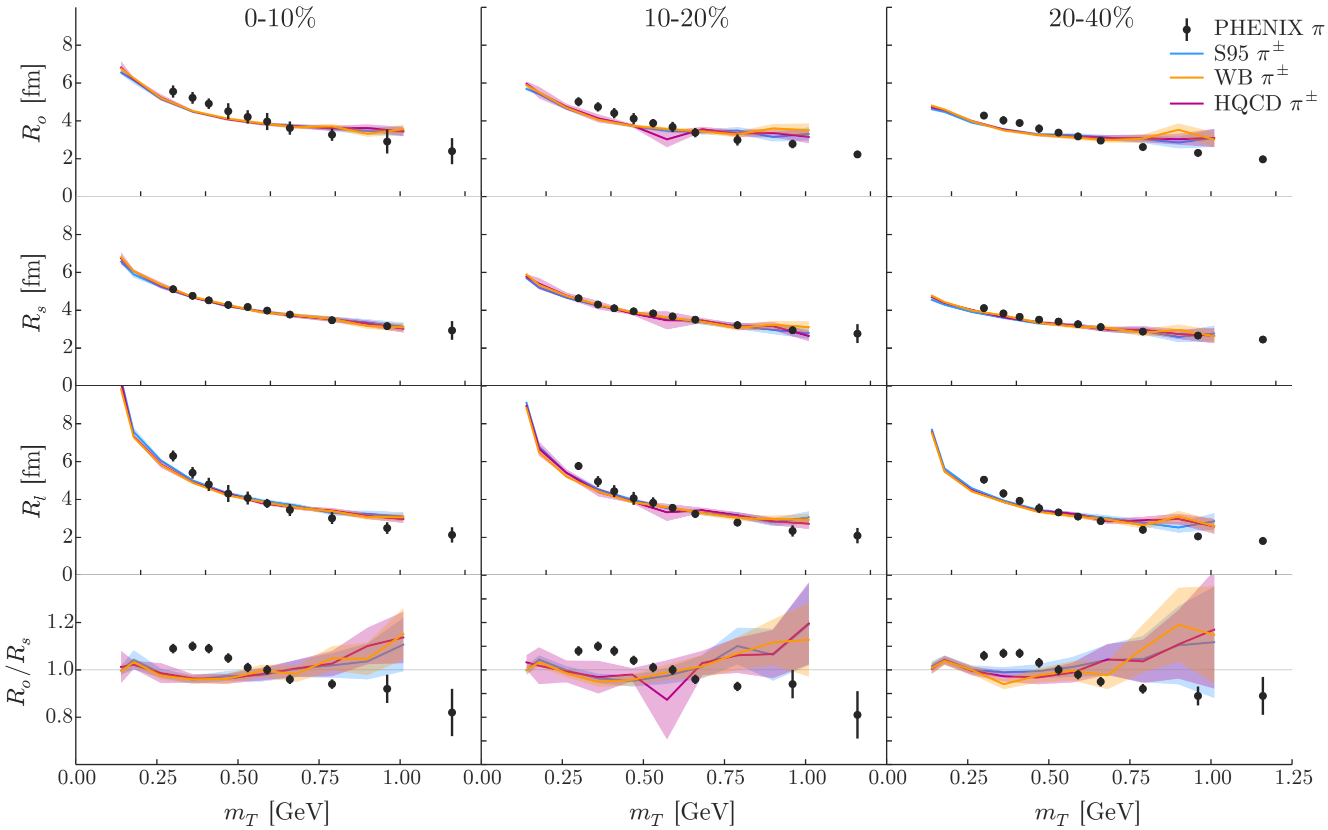

FIG. 7. Effect of the equation of state on the Bertsch-Pratt radii. We plot R_o, R_s, R_l and the ratio R_o/R_s (rows top to bottom) in centrality bins 0–10%, 20–30% and 40–50% (columns left to right) against transverse mass m_T for the HotQCD', WB' and S95' equations of state (purple, orange and blue lines). Shaded bands indicate two sigma errors estimated from the Jacobian of the fit function (21). Symbols with errors bars are experimental data from PHENIX.

the HotQCD' equation of state. This is consistent with previous findings that the S95' equation of state is considerably softer in the vicinity of the phase transition as evidenced by the speed of sound in Fig. 3.

In Fig. 6, we see that the effect on the triangular flow is similar to the effect observed on the elliptic flow except more pronounced and generates as large as a 20% discrepancy in the peripheral flows predicted by the HotQCD' and S95' equations of state. This sensitivity of higher harmonics to the softness of the QGP phase equation of state puts the relatively large higher-order anisotropic flow coefficients observed at RHIC and the LHC into perspective.

C. Femptoscopic Bertsch-Pratt radii

The size of the fireball emission region is estimated using Hanbury-Brown-Twiss (HBT) interferometry for identical particles. The azimuthally averaged two-particle correlation function

$$C(q,k) = \frac{\sum\limits_{n}\sum\limits_{i,j} \delta_q\, \delta_k \Psi(q,r)}{\sum\limits_{n}\sum\limits_{i,j'} \delta_q\, \delta_k} \tag{20}$$

consists of a numerator with particles pairs sampled from the same event and a denominator with pairs sampled from different events. Here $q = p_i - p_j$ denotes the relative momentum, $r = x_i - x_j$ the relative separation and $k = (p_i + p_j)/2$ the average momentum of the pion pair in the longitudinal co-moving frame where the compononent of k along the beam axis vanishes. The numerator is summed over all events n in a given centrality class and unique particle pair combinations i, j in each event. In the denominator, particle i is taken from one event and particle j' from a random partner event in the same centrality class. The delta functions δ_q and δ_k are 1 if the momenta q and k fall into their respective bins and 0 otherwise. Bose-Einsten correlations, which are not included natively in the UrQMD model, are imposed by adding the symmetrization factor $\Psi(q,r) = 1 + \cos q\, r$.

The average pair momentum k is then projected into its longitudinal component k_{z} and transverse component

k_T, while the separation momentum q is represented in the orthogonal coordinates (q_o, q_s, q_l), where q_l lies along the beam axis, q_o is parallel to k_T and q_s perpendicular to q_o and q_l. The resulting correlation function is approximated using a Gaussian source and fit to the parametric form

$$C(q_o, q_s, q_l, k_T) = \mathcal{N}\left(1 + \lambda\, e^{-R_o^2 q_o^2 - R_s^2 q_s^2 - R_l^2 q_l^2}\right) \quad (21)$$

by finding the best fit normalization $\mathcal{N}$, source strength λ and Bertsch-Pratt radii R_o, R_s and R_l for a given transverse momentum k_T.

We calculate the Bertsch-Pratt radii for each equation of state using identical pions. The fit is perfomed using $2 \cdot 10^4$ hydrodynamic events in each centrality bin and an additional 10 UrQMD oversamples per event. The oversamples are then concatenated into a single particle list to increase the number of particle pairs by a factor 10^2.

In Fig. 7, we plot the Bertsch-Pratt radii for the HotQCD', WB' and S95' equations of state as functions of the transverse mass $m_T = \sqrt{m^2 + k_T^2}$. The horizontal rows show the radii R_o, R_s, R_l and ratio R_o/R_s (top to bottom), while the columns mark centrality classes 0–10%, 10–20% and 20–40% (left to right). The different colored lines annotated in the legend indicate different equations of state and the bands estimate the error from the Jacobian of the fit. The symbols with error bars are experimental data from PHENIX.

We see that the Bertsch-Pratt radii predicted by the hybrid model provide a good description of the data across all centralities, except for at low p_T where R_o and R_l slightly undershoot the data. However, in contrast to spectra and flows we see no discernible difference in the Bertsch-Pratt radii predicted by the three different equations of state. This suggests that femptoscopic measurements are not sensitive enough to resolve small differences in the lattice equation of state.

D. HotQCD errors

As a final test we analyze errors in the

V. CONCLUSION AND OUTLOOK

ACKNOWLEDGMENTS

JSM acknowledges support by the DOE/NNSA Stockpile Stewardship Graduate Fellowship under grant no. DE-FC52-08NA28752.

[1] P. Huovinen and P. Petreczky, Nucl. Phys. **A837**, 26 (2010), arXiv:0912.2541 [hep-ph].

[2] P. Huovinen, Nucl. Phys. **A761**, 296 (2005), arXiv:nucl-th/0505036 [nucl-th].

[3] A. Bazavov *et al.* (HotQCD), Phys. Rev. **D90**, 094503 (2014), arXiv:1407.6387 [hep-lat].

[4] S. Borsanyi, Z. Fodor, C. Hoelbling, S. D. Katz, S. Krieg, and K. K. Szabo, Phys. Lett. **B730**, 99 (2014), arXiv:1309.5258 [hep-lat].

[5] A. Bazavov *et al.*, Phys. Rev. **D80**, 014504 (2009), arXiv:0903.4379 [hep-lat].